Article

Laser-Induced Graphene on Optical Fibre: Towards Simple and Cost-Effective Electrochemical/Optical Lab-on-Fibre Bioplatforms

Laura L. Ferreira, Rafael A. Ribeiro, António J. S. Fernandes [ID], Florinda M. Costa [ID], Carlos Marques [ID] and Nuno F. Santos *[ID]

i3N and Department of Physics, University of Aveiro, 3810-193 Aveiro, Portugal; lauraferreira@ua.pt (L.L.F.); rafa.ribeiro@ua.pt (R.A.R.); toze2@ua.pt (A.J.S.F.); flor@ua.pt (F.M.C.); carlos.marques@ua.pt (C.M.)
* Correspondence: nfsantos@ua.pt

Abstract: A 3D graphene foam made of interconnected multilayer graphene flakes was produced on optical fibres (OF) by laser-induced transformation of a polyimide (PI) film coated on the OF cladding. This material, known as laser-induced graphene (LIG), was explored in the electrochemical detection and quantification of dopamine (DA) at physiologically relevant concentrations in the presence of the most relevant interfering molecules in biological fluids, ascorbic acid (AA) and uric acid (UA). The measured limit of detection is 100 nM, the linear range is 0.1 to 5.0 µM and a maximum sensitivity of $5.0 \, \mu A \, \mu M^{-1} \, cm^{-2}$ was obtained for LIG decorated with Pt nanoparticles (NPs). Moreover, immunity to AA and UA interference and to fouling was attained by decorating the LIG electrode with Pt NPs and coating it with Nafion. These figures of merit underline the potential of these sensors for the quantification of physiologically relevant concentrations of DA in biological fluids, paving the way for the development of hybrid electrochemical/optical sensing actuating platforms in a lab-on-fibre configuration, with relevant applications in biomedical engineering. The advantages of this hybrid arrangement include the possibility of in situ counterproofing, extended measuring ranges, photoelectrochemical detection and the probing of inaccessible places. This elegant approach can also provide a simple and cost-effective way to fabricate biomedical devices with extended functionality, such as medical optical probes with added electrochemical capabilities and optogenetics combined with local electrochemical detection, among others.

Keywords: 3D graphene; laser processing; laser-induced graphene; optical fibre; electrochemical sensors; dopamine

1. Introduction

Electrochemical (EC) transducers need to provide high charge transfer rates, low background currents, ease of functionalization and a wide EC window, justifying the increasing interest in the nanoallotropic forms of carbon for this purpose [1–3]. However, the rapid, facile, reproducible and low-cost synthesis of many nanocarbons is still very difficult, involving multiple-step protocols, hindering its widespread application. Furthermore, their miniaturization is difficult, delaying the production of compact multiplexed devices for the simultaneous detection of multiple biomarkers in minimal sample volumes. Among nanocarbons, graphene is especially appealing for EC biosensors due to its unique charge transport characteristics combined with low dimensionality (comparable to most biomolecules) and superior EC performance [4,5], allowing analyte detection at the ng/mL range or even lower [6]. Its low-cost and controlled synthesis is still a challenge in many cases but a new process was developed to obtain a 3D porous graphene-based material on a polymer sheet via IR, VIS or UV laser beam irradiation of polyimide (PI) sheets at atmospheric conditions, known as laser-induced graphene (LIG) [7]. LIG is electrically conductive, flexible, easy and cheap to produce, and amenable to mass production.

Miniaturized patterns can be formed during synthesis avoiding the need for posterior lithographic processing. Besides PI, this method also permits graphene synthesis directly on unconventional substrates such as cork [8], paper [9], wood and even food [10], constituting an interesting alternative for device development on sustainable and low-cost materials that usually are not compatible with standard microfabrication techniques. LIG-based biosensors have been extensively studied in the last years and many articles highlight their merits in this regard [5,11–13]. In general, it is pointed out that the relatively low sheet resistance of a few tens of Ω/sq, the large surface area provided by the porous arrangement of interconnected graphene flakes, and the graphene electrocatalytic activity towards many EC processes, turn LIG into a high-performance material when it comes to lower limits of detection (LoD) and augmenting sensitivity for a wide variety of analytes.

On the other hand, optical fibres (OFs) have also been applied to biosensing, mainly exploring surface plasmon resonance (SPR) employing metal nanofilms or nanoparticles (NPs) [14–17]. Their flexibility, small diameter and low weight combined with immunity to electromagnetic interference, remote sensing capabilities, multi-point and multiplexing capacity are crucial for probing very small or inaccessible places, or conditions where EC sensors alone are unreliable. Indeed, pure EC sensors suffer from electromagnetic noise and interference in chemically complex matrices that affect their performance at low analyte concentrations [16], also requiring precise pH and temperature data for quantification.

The above considerations raise the interest in combining both approaches into a synergistic hybrid device for a lab-on-fibre approach that could carry interest for biomedical applications. The advantages in terms of sensing include a broadened applicability, namely in hard-to-reach places, multiparametric monitoring (biomarkers, temperature, pH, among others), in situ optical/EC counterproofing, and complementary detection ranges provided by the dual mode; all these contained in multiplexed "smart" OFs. Although some fundamental studies with ITO [18,19] and sputtered Au [16] electrodes on OFs have been reported, these hybrid sensors remain relatively unexplored. In the literature, Au-coated OFs were applied to the coupled EC/SPR detection of trace lead ions [16] with improved selectivity and lower LoD compared to standard chromatography or EC sensors. Last, but not least, such a hybrid arrangement would allow the use of one signal type as excitation and the other as detection, covering a wide range of options.

Concerning LIG on OF, Hou et al. have shown that LIG scribed on PI-coated hollow core OF can be used efficiently as a relative humidity sensor [20]. Recent work by our group [21] has shown that LIG produced on PI-coated OFs does not interfere with the intrinsic optical spectral characteristics of sensors inscribed in the OF core but increases its refractive index sensitivity, which is very useful for biosensing applications. LIG on OF can be produced at lower costs compared with other electrode materials used in conjunction with OFs, such as sputtered Au and ITO, whilst minimizing the use of scarce, unsustainable or toxic nanomaterials. However, the EC functionality of LIG on OF is still to be demonstrated.

In this work, we show the state-of-the-art performance of LIG sensors laser-scribed on OFs on the non-enzymatic EC detection and quantification of dopamine (DA), an important neurotransmitter and hormone controlling or affecting several body functions and processes. DA is a catecholamine that plays a significant role both as a neurotransmitter and as a hormone, actuating in the cardiovascular, central nervous, renal and hormonal systems [22]. It is deeply related to motor skills, pleasure, motivation and reward sensations, as well as to humor and learning mechanisms. Several behavioral and medical conditions are related to DA deficiency or surplus, such as neuroendocrine tumors, hypertension or cardiac insufficiency, drug abuse, Parkinson, Alzheimer, schizophrenia, stress or depression [22]. It is thus unsurprising that DA is monitored in in vivo studies in order to better understand its physiological roles as well as to study the process of specific drug development.

In the present study, it was shown that LIG sensors on OFs quantify DA at physiologically relevant concentrations and provide excellent electroanalytical performance,

comparable to LIG produced in PI sheets. This work paves the way for affordable bio plat-forms in a lab-on-fibre configuration capable of synergistic label-free EC-optical operation and sets a framework for further development.

2. Materials and Methods

2.1. Materials and Reagents

The PI-coated OFs were of the type SM1500(4.2/125)P.001, acquired from Fibercore (SMF with 4.2 μm of core diameter, 125 μm total diameter and 30 μm PI coating thick-ness). Silver ink (Electrodag 1415) was obtained from Agar Scientific, as was the insulating resin (Lacomit). Pt NPs aqueous dispersion (3 nm, 99.99%, 1000 ppm in H_2O), Potassium hexacyanoferrate(II) trihydrate (>99%) and Nafion 117 solution (5% in a mixture of lower aliphatic alcohols and H_2O) were supplied from Merck, and DA hydrochloride (>99%), uric acid (>99%) and ascorbic acid (>99.7%) were purchased from Alfa Aesar. Phosphate Buffer Saline (PBS) tablets (pH = 7.4, 1 tablet per 200 mL provides a solution with 0.137 M NaCl, 0.027 M KCl and 10 mM of phosphate buffer) were acquired from Fisher Bioreagent. Deion-ized (DI) water was obtained from a MilliQ water purification system, with a resistivity of 18.2 MΩ.cm. All reagents were used as received without further purification steps.

2.2. Synthesis Apparatus and Electrode Fabrication

In order to produce LIG on OFs, a continuous M500 CO_2 laser (Redsail Technology Laser Co. Ltd, Shandong, China) with a wavelength of 10.6 μm and maximum power output of 60 W was used. The laser beam exits through a laser head that can move linearly in an *xy* plane, so it can pattern any kind of 2D design on the substrate, in this case, a silica OF coated with PI (Figure 1A). The scribing movement is conditioned by several adjustable parameters, such as the spacing between consecutive lines of laser scribing (d), scanning speed (v_{laser}), and laser power (P). In this work, d = 0.08 mm and v_{laser} = 150 mm s^{-1} were used for all LIG electrodes. The laser scanning was carried out transversely to the OF axe. Since the PI irradiated in this case is not a sheet but rather a coating surrounding the OF, a platform that straps and rotates the OF in its longitudinal axis was employed in order to produce LIG all around the OF circumference. The OF was rotated by 90° before each laser irradiation. A power meter (S350C model from Thorlabs) was used to measure the optical power from the laser. The distance between the laser head and the OF was equal to the laser head lens focal length at 1.8 cm (in focus operation).
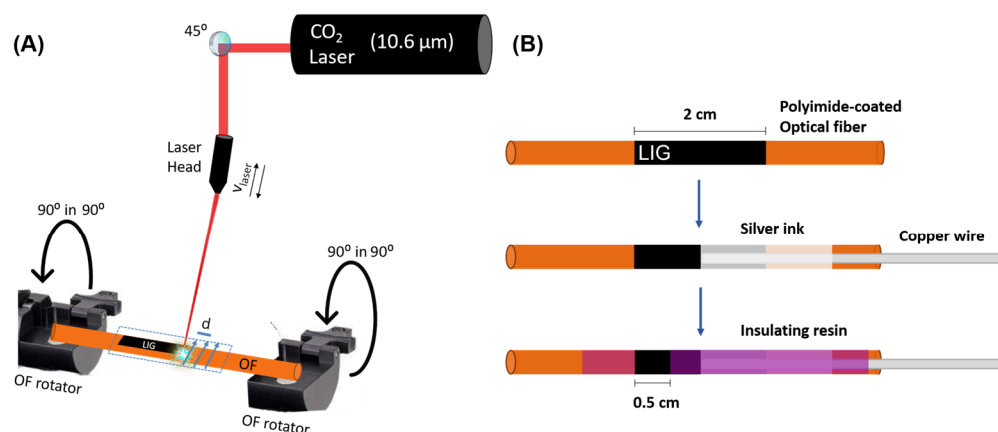
Figure 1. Schematics of (**A**) LIG scribing procedure on OFs and (**B**) LIG electrode assembly on OFs.

Following LIG production, the OFs were thoroughly rinsed in DI water, left to dry overnight and electrical contacts were subsequently established (Figure 1B). The final LIG electrode exhibits 0.5 cm in length, corresponding to ~0.196 cm^2 of exposed active area.

Pt NPs and a Nafion selective membrane were employed seeking enhanced DA sensi-tivity and selectivity against the most problematic interfering molecules in biological fluids, namely ascorbic acid (AA) and uric acid (UA). Pt NPs deposition on the electrochemically

active area of LIG was accomplished by dropcasting 100 µL of Pt NPs aqueous dispersion with a micropipette and letting it evaporate overnight. Nafion deposition was performed by dipcoating the OFs in Nafion 117 solution for 10 s followed by evaporation overnight.

2.3. Morphological, Structural and Elemental Characterization

Scanning electron microscopy (SEM) images were acquired using a Vega 3SB instrument (TESCAN, Brno, Czech Republic), in the secondary electron mode, at high voltages of 25 keV. Energy-dispersive X-ray spectroscopy (EDX) spectra were acquired to identify chemical elements and impurities present on laser-irradiated OFs, as well as to verify if Pt NPs were successfully dropcasted and adsorbed by LIG electrodes. Room temperature micro-Raman spectra were acquired via a Jobin Yvon HR800 instrument (Horiba, Kyoto, Japan), using the retro dispersion configuration, with a He-Cd laser (Kimmon, Tokyo, Japan) with a wavelength of 442 nm and 1 mW power. The laser beam was focused on the OFs using a long-focus distance objective (Olympus, 50×, 0.5 NA). A neutral-density filter was used to avoid modification of graphene with light intensity, as it reduces the laser intensity in all wavelengths. The LIG OFs were placed, one at a time, in a xy-plane holder. Between spectrum acquisitions, the cylindrical LIG OF was rotated manually 180° (turned upside down) so that two different parts of the LIG coating around the OF could be checked for uniformity and overall quality. A 600 groove/mm grating was used to disperse the radiation to the Peltier-cooled CCD sensor. Gauss–Lorentz functions were employed for the fitting of Raman bands using the Labspec software.

2.4. Electrochemical Characterization and Dopamine Electroanalysis

EC measurements were conducted via a Versastat 3 potentiostat/galvanostat (Princeton Applied Research, Oak Ridge, TN, USA). A three-electrode setup was employed using a homemade 3D printed cell, where LIG on OFs were the working electrode (WE), a platinum wire the counter electrode (CE) and a standard calomel electrode (SCE, 3.9 M KCl) the reference electrode (RE). The OFs were placed through the orifices of the cell lid so that they could be suspended and dipped 3.5 cm in the electrolyte solution. For EC characterization via cyclic voltammetry (CV) measurements, the electrolyte solution consisted of 5 mM of potassium ferrocyanide—$[Fe(CN)_6]^{4-}$—as the active redox probe, in a 50 mL of Phosphate Buffer Saline (PBS) solution with pH = 7.4. All measurements were performed inside a Faraday cage.

Differential pulse voltammetry (DPV) was employed for DA electroanalysis in the presence of AA and UA interferents. In DPV, short and small amplitude potential pulses are superimposed on a linear DC potential sweep constituted of small discrete steps. The current is measured right before and at the end of the potential pulse and the differential current is calculated. Contrary to CV where no pulses are superimposed on the linear potential sweep, DPV allows for the reduction of background currents arising from the linear potential sweep. This results in much better discrimination of faradaic currents (as the ones resulting from DA oxidation) from capacitive ones, thus lowering the limits of detection. DPV peaks are also narrower than oxidation waves in CVs, permitting much better discrimination among different electroactive species (DA, AA and UA) and thus enhanced selectivity. Two distinct sets of DPV parameters were studied in DA-PBS solution (see Table 1) and ultimately the set of conditions providing lower LoD was chosen for further studies. For all the EC measurements, the electrolyte volume was 35 mL. A preconcentration step to boost sensitivity towards DA was employed in order to explore the different charge states of DA and AA/UA interferents. Prior to the DPVs, the electrodes were conditioned in PBS buffer by cycling the potential in the −1 to 1 V window at 50 mV s^{-1} for 20 cycles.

Table 1. Differential pulse voltammetry (DPV) parameters for DA electroanalysis.

|	DPV#1	DPV#2
Preconcentration time/potential	3 min/-0.3 V vs. SCE	
Initial; Final Potential (V)	-0.2; 0.6	-0.2; 0.6
Scanning Speed (mV s^{-1})	10	10
Pulse: height (mV); width (s)	45; 0.03	30; 0.15
Step: height (mV); width (s)	2; 0.2	3.5; 0.35

3. Results and Discussion

3.1. Morphological, Structural and Electrochemical Characterization

Figure 2 shows the SEM images of PI-coated OFs processed at two different laser powers, 2.5 W and 4 W. At 2.5 W, it is possible to observe two different morphologies. Pinpointed areas highlighted by a yellow arrow in Figure 2A, show a porous structure with a 3D arrangement of graphene multi-layers, characteristic of LIG, as confirmed by Raman spectroscopy, Figure 3. However, this transformation of PI into LIG is not uniform, as some areas pinpointed in red that appear in between them do not present the typical microstructure of LIG (Figure 2B). Thus, 2.5 W lasing power for the specific focusing conditions and scribing system employed in this study seems to be close to the threshold lasing power to attain the photothermal conversion of PI into LIG. In contrast, LIG formed at 4 W laser power denotes superior homogeneity and all PI has been transformed into a laminated and porous microstructure (Figure 2C,D). This is corroborated by cross-section imaging of Figure 2E, showing LIG formed all around the OF circumference and deep into the cladding interface. No unprocessed PI appears between the LIG layer and the OF cladding. It is thus clear that increasing the lasing power from 2.5 to 4 W increases the overall LIG homogeneity and overall porosity, in accordance with previous findings on these matters [23].
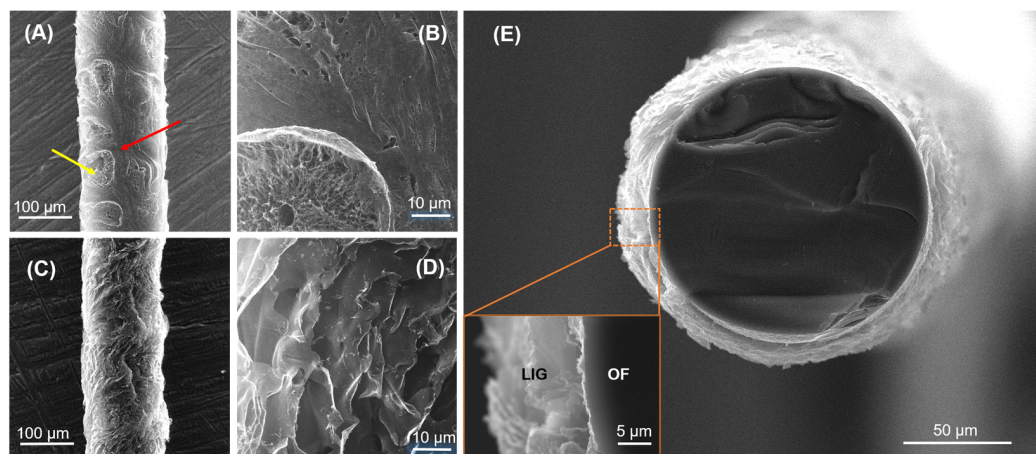
Figure 2. SEM micrographs of LIG scribed on OFs at (**A**,**B**) 2.5 W and (**C**–**E**) 4 W.

Raman spectroscopy was used to compare the structural quality of the LIG electrodes processed under 2.5 and 4 W lasing powers, and representative results are shown in Figure 3. The Raman spectra of LIG are dominated by the D, G and 2D (D overtone) bands, along with some other smaller bands, D' and 2D', as well as the combined overtones D + D' and D + D''. The G peak at ~1580 cm^{-1} corresponds to phonon scattering of the stretching mode of the sp^2 carbon bonds (E$_{2g}$ vibrational mode), indicating graphitization. The 2D overtone at ~2740 cm^{-1} refers to the scattering of two Brillouin zone boundary phonons, with symmetric momenta, of the breathing modes of perfect aromatic rings. For single-layer graphene (SLG), the 2D peak is very sharp, symmetric and has increased intensity,

compared to bilayer or few-layer graphene, where the peak will broaden and shift in position as well [24]. The ratio between the 2D and G bands, I_{2D}/I_G, allows the qualitative inference of the number of graphene layers present in LIG. A $I_{2D}/I_G \approx 2$ is a usual feature for SLG [24], whereas in LIG, that ratio is about 0.3 to 0.4 and the 2D band is significantly broadened, indicating the presence of uncorrelated multilayer graphene.
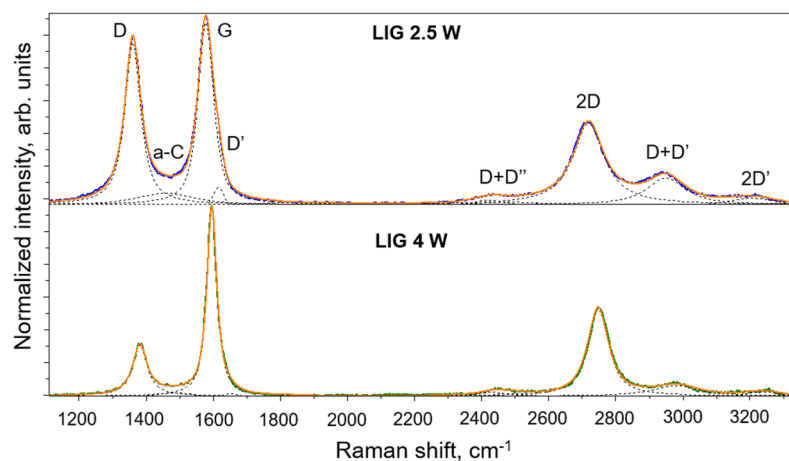
Figure 3. Raman spectra of LIG produced at (**top**) 2.5 W and (**bottom**) 4 W on OFs. The spectra were background-subtracted and normalized to the G band intensity and shifted in intensity for clarity. Fitted Gauss-Lorentz shapes are shown in black dashed lines and the respective sum is in solid orange lines.

The D band at ~1370 cm^{-1}, not allowed by momentum selection rules in pure graphene, arises from one-phonon scattering involving the breathing mode of aromatic rings, requiring defective or bent sp^2 carbon bonds for its activation [25]. Its presence, therefore, indicates a significant concentration of defects in the graphene structure. Along with the D and G band full width at half-maximum (FWHM), the I_D/I_G ratio can be used to study structural aspects of the multilayer graphene. The I_D/I_G ratio scales with disorder for sp^2 phases obeying the Tuinstra–Koenig relation, valid for sp^2 carbon phases presenting well-defined and intense G bands at ~1580–1590 cm^{-1} [26]. Clearly, both the D and G bands' FWHM and the I_D/I_G ratio are larger for LIG produced at 2.5 W (57 cm^{-1} and 55 cm^{-1} for the D and G band FWHM, respectively, and an I_D/I_G ratio of 0.89) compared to LIG produced at 4 W (52 cm^{-1} and 36 cm^{-1} for the D and G bands' FWHM, respectively, and an I_D/I_G ratio of 0.27), clearly indicating that the latter presents lower defect density and higher crystallinity. Moreover, the a-C band at ~1450–1500 cm^{-1}, related to the presence of amorphized carbon phases, is much more intense for LIG produced at 2.5 W. This analysis corroborates the SEM observations suggesting that 2.5 W laser power is indeed near the threshold for LIG formation since, at lower laser powers, only amorphized carbon phases are produced instead of LIG. Note that the spectrum presented for 2.5 W LIG corresponds to the regions indicated by the yellow arrow in Figure 2A. Raman spectra acquired from the regions pinpointed by the red arrows (not shown) still denote the typical fingerprint of LIG, though the bands are further broadened and the I_{2D}/I_G intensity ratio is typically lower.

These differences in terms of morphology and structure are obviously reverberated into the EC response of each. This is clearly seen in the cyclic voltammetry studies of Figure 4 employing a standard, "well-behaved" probe, [Fe(CN)$_6$]$^{3-/4-}$ in PBS buffer.
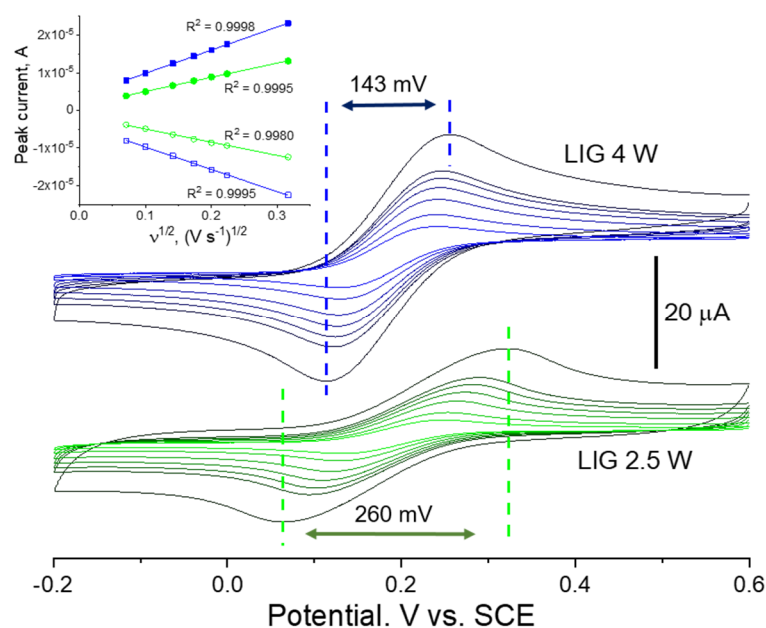
Figure 4. Cyclic voltammograms at selected scan rates (from light green/blue to dark green/blue: 5, 10, 20, 30, 40, 50 and 100 mV s^{-1}) using 5 mM [Fe(CN)$_6$]$^{4-}$ in PBS for (top, blue lines) 4 W LIG and (bottom, green lines) 2.5 W LIG on OFs. The inset shows the evolution of peak anodic and peak cathodic currents with the square root of the potential scan rate for 4 W LIG (blue squares) and 2.5 W LIG (green circles) electrodes.

For both 4 W and 2.5 W LIG on OFs, the redox waves are well-defined and the current response increases with increasing scan rates as expected. Faster scan rates provide less time for reactions to take place at the electrode's surface and decrease the diffusion layer thickness, which in turn increases the mass transport of ions and the current signal [27]. Specifically, for a one-electron reversible electron transfer process limited by a semi-infinite diffusion regime, the peak current i$_p$ (A) is linearly proportional to the square root of the scan rate ν (V s^{-1}), according to the Randles-Ševčík relation (at 25 °C) [27].

$$i_p = 0.269A_{eff}C(D\nu)^{\frac{1}{2}} \tag{1}$$

where C (mM) is the [Fe(CN)$_6$]$^{4-}$ bulk concentration in mM (5 mM), A$_{eff}$ (cm^2) is the electrode's electrochemically active area, and D (cm^2 s^{-1}) is the [Fe(CN)$_6$]$^{4-}$ diffusion coefficient in aqueous solution [28] (6.66 × 10^{-6} cm^2 s^{-1}). This is clearly the case for both 2.5 W and 4 W LIG in the studied range of scan rates, for which the anodic and cathodic peak currents show a symmetric linear dependence with the square root of the scan rate, with all fittings having a coefficient of determination R^2 above 0.998 (see inset of Figure 4). The voltammograms differ, however, in the magnitude of peak currents and in the separation of the anodic and cathodic peak potentials. Indeed, as exemplified for 100 mV s^{-1}, LIG produced on OFs at 4W LIG maintains a 143 mV peak-to-peak separation, about 120 mV less than LIG produced at 2.5 W lasing power. This undoubtedly indicates that the 4 W material is characterized by faster electron transfer kinetics compared to that of 2.5 W. The electrochemically active area can be derived via the slope of the linear regression of anodic branches and via equation 1, resulting in 1.09 mm^2 and 1.78 mm^2 for the 2.5 W and 4 W LIG electrodes, respectively, for a geometrical exposed area of c.a. 1.96 mm^2. The severely diminished active area of the 2.5 W LIG electrode compared to the geometrical area is in accordance with the analysis of LIG morphology in Figure 2. These results indicate that LIG electrodes produced at 4 W present superior EC characteristics for biosensing purposes and were thus selected for the detection and quantification of DA.

3.2. Dopamine (DA) Electroanalysis

DA is easily electro-oxidized into dopamine-o-quinone ($C_8H_9NO_2$), in a two proton-2 electron reversible reaction:

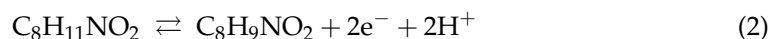$$C_8H_{11}NO_2 \rightleftarrows C_8H_9NO_2 + 2e^- + 2H^+ \tag{2}$$

Figure 5 shows differential pulse voltammetry (DPV) measurements in DA-containing PBS buffer after blank baseline subtraction. DA oxidation reaction (Equation (2)) peaks at about 0.15 V vs. SCE. It is clear that the LIG electrodes produced at 4W laser power permit higher DA oxidation currents when compared to their 2.5 W counterparts. In addition, for both DPV parameter sets tested (see Table 1), the signal-to-noise ratio is higher for 4W LIG. Hence, lower LoD and higher sensitivity are attained for these sensors. This is in agreement with the arguments of the previous morphological, structural and EC characterization using ferro/ferricyanide redox probes. The conductive and highly porous 3D graphene arrangement obtained at 4W lasing power provides high surface area and fast charge transfer for reversible redox reactions to take place. On the contrary, at 2.5 W laser power a non-homogeneous and amorphized graphene phase is obtained with an obvious impact on charge transfer kinetics and electroanalytical capabilities.
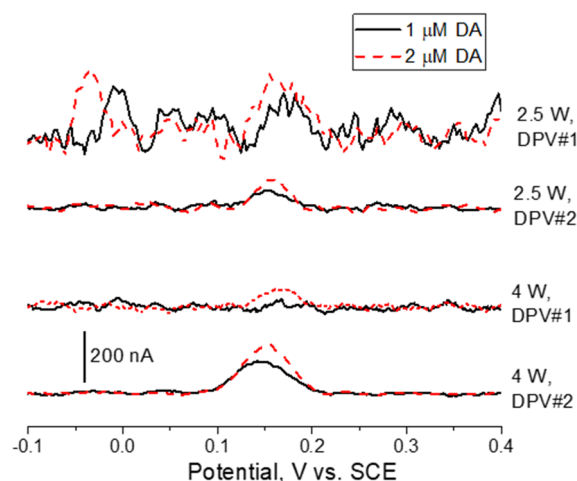
Figure 5. Background-subtracted DPV scans showing DA electro-oxidation in PBS for 2.5 W and 4 W LIG electrodes scribed on OFs and for different DPV parameters (see DPV#1 and DPV#2 in Table 1).

As regards the two different parameter sets for DPV, it is clear that DPV#2 allows for both higher differential currents and signal-to-noise ratio. The combination of 2.5 W lasing and DPV#1 hampers DA detection at 2 µM, whereas 4W lasing plus DPV#2 allows for a clear DA oxidation wave at 1 µM. The last set was therefore employed for the subsequent DA quantification tests.

Other molecules present in biological fluids at relevant concentrations, such as ascorbic acid (AA) and uric acid (UA), are also electrooxidized at electrode potentials that can interfere with the DA electrooxidation, either directly by overlapping oxidation waves or indirectly via undesired interactions of AA/UA interferents (or their oxidation by-products) with DA. Uric acid ($C_5H_4N_4O_3$) is electrooxidized into diimide quinonoid ($C_5H_2N_4O_3$) according to

$$C_5H_4N_4O_3 \rightleftarrows C_5H_2N_4O_3 + 2e^- + 2H^+ \tag{3}$$
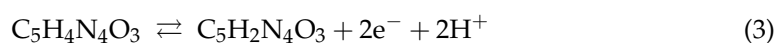
On the other hand, ascorbic acid ($C_6H_8O_6$) is electrooxidized into dehydroascrobate ($C_6H_6O_6$), also a two proton-two electron process:

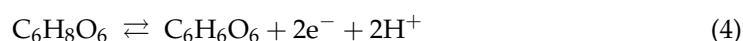$$C_6H_8O_6 \rightleftarrows C_6H_6O_6 + 2e^- + 2H^+ \tag{4}$$

Figure 6 shows the DPV measurements in PBS (pH 7.4) employing LIG electrodes on OFs. Importantly, regardless of the electrode architecture employed (LIG, LIG/Pt NPs and LIG/Pt NPs/Nafion), the measured LoD is 100 nM, which is adequate for measuring DA in several biological fluids, such as in urine (maximum reference value for a "healthy" adult of 3300 nM/24 h) [29] or abnormal concentrations in extracellular fluid (>c.a. 100 nM) [30]. The measured LoDs are inclusively similar to those found for LIG produced on PI sheets (see Table 2). Sensitivities are comparable to other LIG sensors produced on PI sheets and employing Pt NPs, although one order of magnitude lower compared to the high record in the literature for PI-LIG [5].
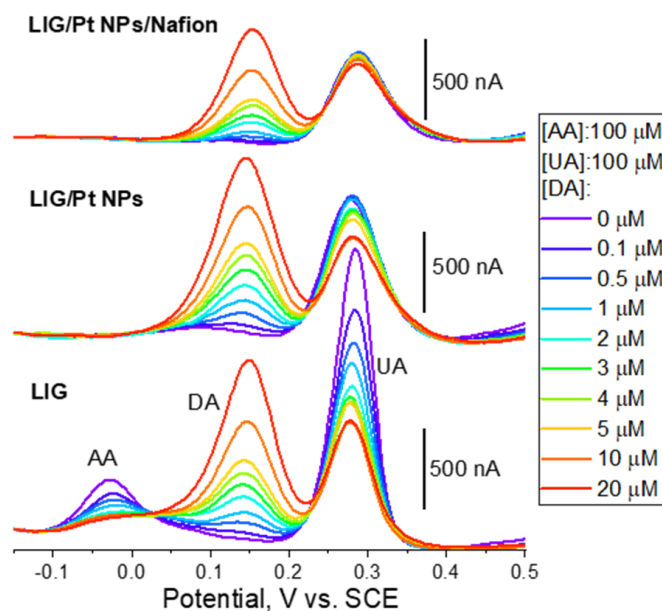
Figure 6. Background-subtracted DPVs of DA, AA and UA ternary mixtures using (bottom to top) LIG, LIG/Pt NPs and LIG/Pt NPs/Nafion electrodes on OFs. AA and UA concentrations are 100 μM each. The DPV parameters employed are the ones labeled DPV#2 in Table 1.

Table 2. Figure of merit of the LIG on OFs dopamine EC sensors and comparison with other LIG non-enzymatic sensors fabricated on PI films.

| Electrode		Linear Range, μM	LoD, μM	Sensitivity, μA μM^{-1} cm^{-2}	[AA]; [UA], μM	$\Delta E_{p, DA-UA}/\Delta E_{p, AA-DA}$, mV	[Ref]
LIG on OF (CO$_2$ laser)	LIG	0.1–5	0.1 (measured)	4.4	AA—100; UA—100	134/168	This work
	LIG/Pt NPs	0.1–5	0.1 (measured)	5.0		137/N.A.	
	LIG/Pt NPs/Nafion	0.1–5	0.1 (measured)	2.6		133/N.A.	
ITO/LIG (CO$_2$ laser)		0.2–24	0.20 (measured)	2.1	AA—10; UA—10	135/155	[31]
LIG (CO$_2$ laser)/Pt NPs		0–30	0.07 (extrapolated)	7.0	AA—30; UA—4	143/236; 134/234 (without Pt NPs)	[32]
LIG (CO$_2$ Laser)		0.5–3	0.50 (measured); 0.10 (extrapolated)	93	AA—100; UA—100	175/190	[5]
LIG (UV laser)		0.5–4	0.50 (measured); 0.13 (extrapolated)	58	AA—100; UA—100	160/190	[5]
LIG (CO$_2$ laser)/ PEDOT		1–150	0.33 (extrapolated)	~2.0	AA—30; UA—4	150/250; 144/171 (without PEDOT)	[33]

AA electrooxidation is usually a less reversible reaction compared to DA and UA. This is readily observed in the DPV using bare LIG electrodes (bottom DPVs in Figure 6), where peak currents for UA oxidation (c.a. 280 mV vs. SCE) are four-fold those of AA oxidation (c.a. -25 mV vs. SCE) for the same concentration (100 μM) and identical to the peak current obtained for DA at a concentration of 4 μM. This underlines the electrocatalytic effect of LIG towards DA oxidation favoring it against AA and UA interferents. This phenomenon has been attributed to the π-π stacking and electrostatic attraction between graphene delocalized π electrons and DA aromatic rings [34,35]. UA also possesses an aromatic ring in its structure, whereas AA does not. Moreover, pyrrolic-N has been shown to be present in LIG samples produced on PI sheets, which can facilitate DA oxidation via hydrogen bonds with the DA hydroxyl or amine groups [36,37]. On the other hand, the negatively charged AA and UA are repulsed electrostatically by graphene, contributing to the natural selectivity of LIG towards DA. Finally, the employed preconcentration step at -0.3 V vs. SCE for 3 min further contributes to this discrimination taking advantage of the opposite intrinsic charge of positive DA molecules and negative AA and UA molecules.

Interestingly, when Pt NPs are dropcasted into the LIG electrode, the DPV profile changes dramatically. Interestingly, AA oxidation wave at c.a. -25 mV disappears so that Pt NPs are effective in preventing direct AA interference in DA quantification. It is important to note that the Pt NPs are dispersed in DI water and dropcasted into LIG surface so this behavior cannot be attributed to any effect related to the interaction of the dispersing media and the LIG surface. In fact, a similar effect has been reported in the literature for reduced graphene oxide decorated with Pt NPs of similar size as used herein [38]. On the other hand, despite a small increase in sensitivity (see Table 2), Pt NPs seem not to induce a decisive enhancement in the electroanalytical response. In fact, DA-UA peak-to-peak separations ($\Delta E_{p, DA-UA}$ in Table 2) remain similar when incorporating Pt NPs as only a small 3 mV increase is observed. These observations contradict the findings of another work where planar LIG/Pt NPs electrodes produced on PI sheets [32] were characterized in AA-DA-UA ternary mixtures. In that work, the incorporation of Pt NPs is seen to improve the electroanalytical response of LIG via a clear enhancement in sensitivity and lower LoD, which is attributed to the remarkable electrocatalytic properties of Pt NPs. Possible explanations for this apparent contradiction may rely on the different sizes of NPs employed, their concentration at the electrode surface, the specific physical properties and surface chemistry of each LIG type and/or dissimilar DPV measurement parameters. The presence of Pt NPs on LIG was assessed via multi-point EDX measurements (not shown) and resulted in an average concentration of 0.42 ± 0.18 at %.

Regarding the bare LIG electrodes, it is clear that, with the successive measurements in AA-DA-UA ternary mixtures, the intensity of the AA and UA peaks are decreasing. It is also clear that despite an initial quasi-linear response of the sensor at lower DA concentrations (Figure 7), a progressive signal saturation occurs. Similar to the findings in the literature regarding LIG on PI sheets [5], this is likely caused by electrode fouling via the deposition of reagent molecules and/or oxidation byproducts. It is widely accepted that DA electrochemical mechanisms and reaction pathways are complex [39]. However, there is also a general agreement in the literature that a chemical step follows the initial electrooxidation step presented in Equation (2), probably a Michael addition of the primary amine group to the aromatic ring [39]. This, in addition to possible intermolecular polymerization reactions, may result in the progressive formation of deposits that partially inactivate the electrode surface, and hence to the diminishing of subsequent oxidation currents. This is readily and especially observable in the bare LIG electrode, where UA and AA oxidation currents are diminished severely as DPVs are performed.

The complexity of DA electrochemistry and the wide variety of electrode materials employed may be the reason why different explanations exist for similar features encountered in DA electroanalysis. For instance, a report in the literature employing ZnO nanowire electrodes states that, at lower concentrations, DA surface coverage proceeds via monolayer adsorption, whereas for higher concentrations, the surface monolayer starts saturating

and secondary multilayer formation occurs [40]. The interaction with the electrode surface by these higher/ranking adsorption layers is partially screened by the former, leading to a change in electrode response into a second linear regime [40]. This surface coverage model is also concomitant with the progressive hindering of AA and UA oxidation waves. A thorough investigation of these matters is out of the scope of this work, where the obtained data points were chosen in order to privilege DA concentrations up to 5 µM as this constitutes the more useful range for clinical and medical applications. The higher concentration range data points are insufficient to check if indeed it constitutes a second linear region.
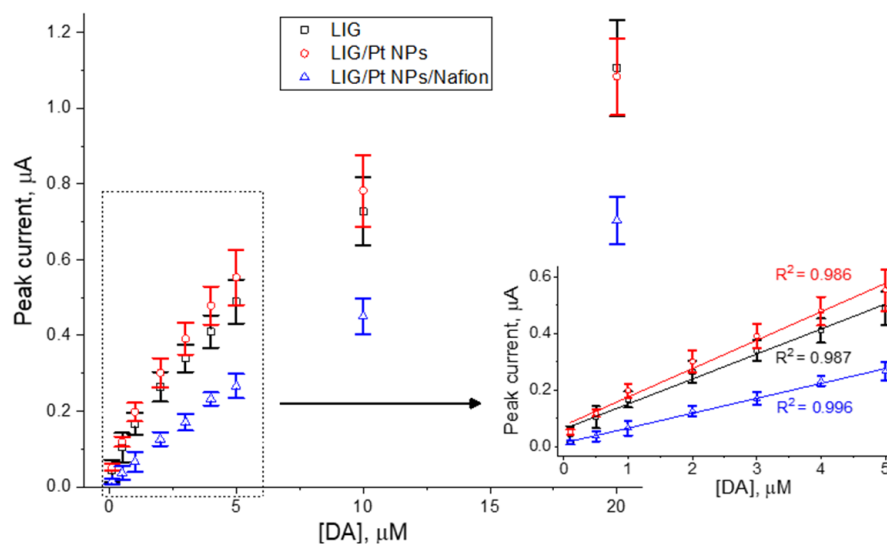
Figure 7. Plot of peak current densities as function of DA concentration for LIG, LIG/Pt NPs and LIG/Pt NPs/Nafion electrodes on OFs. Error bars are statistics from independent triplicate measurements. The inset shows linear regressions for each electrode type.

When Nafion, an anionic polymer, is dropcasted on top of the LIG/PtNPs-coated OFs, further changes to the electroanalytical response are observable. Sensitivity to DA is lowered compared to LIG/Pt NPs, which is expected due to the presence of Nafion. Despite being permeable to cationic forms (such as DA), it still constitutes a physical barrier to the diffusion of DA. On the other hand, the UA oxidation wave is still visible in a ratio to the DA wave similar to the case of the LIG/Pt NPs. This is somewhat unexpected since UA is negatively charged at pH 7.4 and its diffusion into the LIG/Pt NPs surface should have been blocked by the anionic polymer. This effect was also observed in the literature when developing uric acid sensors [41]. In both cases, one possible explanation could lie in the insufficient Nafion coverage of the sensor surface, which is especially prone to occur in highly porous materials such as LIG. It is, however, interesting to note that, especially up to 5 µM DA, UA oxidation currents are much more stable compared to the remaining, and a higher coefficient of determination ($R^2 = 0.996$) of the DA calibration curve is achieved. This indicates that, in this concentration range, fouling is being suppressed by the use of Nafion, which is of extreme relevance if continuous and long-term measurements are intended.

4. Conclusions

Laser-induced graphene produced photothermally on optical fibers via CO_2 laser irradiation of polyimide-coated OFs is suitable for dopamine electroanalysis considering the physiological ranges of interest. The measured LoD of 100 nM and minimization of fouling effects and interference from ascorbic acid and uric acid via deposition of Pt NPs and Nafion are adequate for in vivo measurements, also taking into account the proven biocompatibility and antimicrobial properties of LIG [42], Pt NPs [43] and Nafion [44]. These results support

further work on the exploitation of these cost-effective hybrid LIG/OF platforms for electrochemical/optical biosensors/bioactuators for a wide variety of scenarios. Possible future applications include fiberscopes employing OF imaging probes with in situ label-free EC capabilities, as well as highly versatile combinations of electrochemistry and optogenetics at high selectivity and usable spatial and temporal resolutions, critical aspects in the study of biologic functions.

Author Contributions: Conceptualization N.F.S.; methodology C.M. and N.F.S.; Formal analysis N.F.S.; results validation N.F.S. and C.M.; investigation L.L.F., R.A.R., A.J.S.F. and N.F.S.; visualization L.L.F., R.A.R. and N.F.S.; Resources N.F.S., C.M. and F.M.C.; writing-original draft by N.F.S.; writing-review and editing L.L.F., R.A.R., F.M.C., A.J.S.F., C.M. and N.F.S.; supervision N.F.S. and C.M.; Project administration F.M.C. All authors have read and agreed to the published version of the manuscript.

Institutional Review Board Statement: Not applicable.

Informed Consent Statement: Not applicable.

Data Availability Statement: Statement data set available with last author.

Conflicts of Interest: The authors declare no conflict of interest.

References

1. Coroş, M.; Pruneanu, S.; Staden, R.-I.S. Review—Recent Progress in the Graphene-Based Electrochemical Sensors and Biosensors. *J. Electrochem. Soc.* **2019**, *167*, 037528. [CrossRef]
2. Santos, N.F.; Pereira, S.O.; Fernandes, A.J.S.; Vasconcelos, T.L.; Fung, C.M.; Archanjo, B.S.; Achete, C.A.; Teixeira, S.R.; Silva, R.F.; Costa, F.M. Physical Structure and Electrochemical Response of Diamond–Graphite Nanoplatelets: From CVD Synthesis to Label-Free Biosensors. *ACS Appl. Mater. Interfaces* **2019**, 8470–8482. [CrossRef] [PubMed]
3. Georgakilas, V.; Perman, J.A.; Tucek, J.; Zboril, R. Broad Family of Carbon Nanoallotropes: Classification, Chemistry, and Applications of Fullerenes, Carbon Dots, Nanotubes, Graphene, Nanodiamonds, and Combined Superstructures. *Chem. Rev.* **2015**, *115*, 4744–4822. [CrossRef] [PubMed]
4. Ambrosi, A.; Chua, C.K.; Latiff, N.M.; Loo, A.H.; Wong, C.H.A.; Eng, A.Y.S.; Bonanni, A.; Pumera, M. Graphene and Its Electrochemistry-an Update. *Chem. Soc. Rev.* **2016**, *45*, 2458–2493. [CrossRef]
5. Santos, N.F.; Pereira, S.O.; Moreira, A.; Girão, A.V.; Carvalho, A.F.; Fernandes, A.J.S.; Costa, F.M. IR and UV Laser-Induced Graphene: Application as Dopamine Electrochemical Sensors. *Adv. Mater. Technol.* **2021**, *6*, 2100007. [CrossRef]
6. Cheng, C.; Wang, S.; Wu, J.; Yu, Y.; Li, R.; Eda, S.; Chen, J.; Feng, G.; Lawrie, B.; Hu, A. Bisphenol A Sensors on Polyimide Fabricated by Laser Direct Writing for Onsite River Water Monitoring at Attomolar Concentration. *ACS Appl. Mater. Interfaces* **2016**, *8*, 17784–17792. [CrossRef]
7. Ye, R.; James, D.K.; Tour, J.M. Laser-Induced Graphene: From Discovery to Translation. *Adv. Mater.* **2019**, *31*, 1803621. [CrossRef]
8. Carvalho, A.F.; Fernandes, A.J.S.; Martins, R.; Fortunato, E.; Costa, F.M. Laser-Induced Graphene Piezoresistive Sensors Synthesized Directly on Cork Insoles for Gait Analysis. *Adv. Mater. Technol.* **2020**, *5*, 2000630. [CrossRef]
9. Kulyk, B.; Pereira, S.O.; Fernandes, A.J.S.; Fortunato, E.; Costa, F.M.; Santos, N.F. Laser-Induced Graphene from Paper for Non-Enzymatic Uric Acid Electrochemical Sensing in Urine. *Carbon* **2022**, *197*, 253–263. [CrossRef]
10. Chyan, Y.; Ye, R.; Li, Y.; Singh, S.P.; Arnusch, C.J.; Tour, J.M. Laser-Induced Graphene by Multiple Lasing: Toward Electronics on Cloth, Paper, and Food. *ACS Nano* **2018**, *12*, 2176–2183. [CrossRef]
11. Simsek, M.; Wongkaew, N. Carbon Nanomaterial Hybrids via Laser Writing for High-Performance Non-Enzymatic Electrochemical Sensors: A Critical Review. *Anal. Bioanal. Chem.* **2021**, *413*, 6079–6099. [CrossRef] [PubMed]
12. Li, G. Direct Laser Writing of Graphene Electrodes. *J. Appl. Phys.* **2020**, *127*, 010901. [CrossRef]
13. Pereira, S.O.; Santos, N.F.; Carvalho, A.F.; Fernandes, A.J.S.; Costa, F.M. Electrochemical Response of Glucose Oxidase Adsorbed on Laser-Induced Graphene. *Nanomater* **2021**, *11*, 1893. [CrossRef] [PubMed]
14. Soares, M.S.; Silva, L.C.B.; Vidal, M.; Loyez, M.; Facão, M.; Caucheteur, C.; Segatto, M.E.V.; Costa, F.M.; Leitão, C.; Pereira, S.O.; et al. Label-Free Plasmonic Immunosensor for Cortisol Detection in a D-Shaped Optical Fiber. *Biomed. Opt. Express* **2022**, *13*, 3259. [CrossRef] [PubMed]

15. Soares, M.S.; Vidal, M.; Santos, N.F.; Costa, F.M.; Marques, C.; Pereira, S.O.; Leitão, C. Immunosensing Based on Optical Fiber Technology: Recent Advances. *Biosensors* **2021**, *11*, 305. [CrossRef] [PubMed]

16. Si, Y.; Lao, J.; Zhang, X.; Liu, Y.; Cai, S.; Gonzalez-Vila, A.; Li, K.; Huang, Y.; Yuan, Y.; Caucheteur, C.; et al. Electrochemical Plasmonic Fiber-Optic Sensors for Ultra-Sensitive Heavy Metal Detection. *J. Light. Technol.* **2019**, *37*, 3495–3502. [CrossRef]

17. Liu, X.; Singh, R.; Li, M.; Li, G.; Min, R.; Marques, C.; Zhang, B.; Zhang, B.; Kumar, S. Plasmonic Sensor Based on Offset-Splicing and Waist-Expanded Taper Using Multicore Fiber for Detection of Aflatoxins B1 in Critical Sectors. *Opt. Express* **2023**, *31*, 4783–4802. [CrossRef]

18. Tramarin, L.; Casquel, R.; Gil-Rostra, J.; González-Martínez, M.Á.; Herrero-Labrador, R.; Murillo, A.M.M.; Laguna, M.F.; Bañuls, M.J.; González-Elipe, A.R.; Holgado, M. Design and Characterization of ITO-Covered Resonant Nanopillars for Dual Optical and Electrochemical Sensing. *Chemosensors* **2022**, *10*, 393. [CrossRef]

19. Niedziałkowski, P.; Białobrzeska, W.; Burnat, D.; Sezemsky, P. Study on Combined Optical and Electrochemical Analysis Using Indium-Tin-Oxide-Coated Optical Fiber Sensor. *Electroanalysis* **2019**, *31*, 398–404. [CrossRef]

20. Hou, M.; Wang, N.; Chen, Y.; Ou, Z.; Chen, X.; Shen, F.; Jiang, H. Laser-Induced Graphene Coated Hollow-Core Fiber for Humidity Sensing. *Sens. Actuators B Chem.* **2022**, *359*, 131530. [CrossRef]

21. Martins, L.; Kulyk, B.; Theodosiou, A.; Ioannou, A.; Moreirinha, C.; Kalli, K.; Santos, N.; Costa, F.; Pereira, S.O.; Marques, C. Laser-Induced Graphene from Commercial Polyimide Coated Optical Fibers for Sensor Development. *Opt. Laser Technol.* **2023**, *160*, 109047. [CrossRef]

22. Liu, X.; Liu, J. Biosensors and Sensors for Dopamine Detection. *View* **2021**, *2*, 20200102. [CrossRef]

23. Duy, L.X.; Peng, Z.; Li, Y.; Zhang, J.; Ji, Y.; Tour, J.M. Laser-Induced Graphene Fibers. *Carbon* **2018**, *126*, 472–479. [CrossRef]

24. Ferrari, A.C.; Meyer, J.C.; Scardaci, V.; Casiraghi, C.; Lazzeri, M.; Mauri, F.; Piscanec, S.; Jiang, D.; Novoselov, K.S.; Roth, S.; et al. Raman Spectrum of Graphene and Graphene Layers. *Phys. Rev. Lett.* **2006**, *97*, 187401. [CrossRef] [PubMed]

25. Ferrari, A.C. Raman Spectroscopy of Graphene and Graphite: Disorder, Electron-Phonon Coupling, Doping and Nonadiabatic Effects. *Solid State Commun.* **2007**, *143*, 47–57. [CrossRef]

26. Tuinstra, F.; Koenig, J.L. Raman Spectrum of Graphite. *J. Chem. Phys.* **1970**, *53*, 1126–1130. [CrossRef]

27. Bard, A.J.; Faulkner, L.R. *Electrochemical Methods: Fundamentals and Applications*; John Wiley & Sons: New York, NY, USA, 1980.

28. Konopka, S.J.; McDuffie, B. Diffusion Coefficients of Ferri- and Ferrocyanide Ions in Aqueous Media, Using Twin-Electrode Thin-Layer Electrochemistry. *Anal. Chem.* **1970**, *42*, 1741–1746. [CrossRef]

29. Davidson, D.F. Elevated Urinary Dopamine in Adults and Children. *Ann. Clin. Biochem.* **2005**, *42 Pt 3*, 200–207. [CrossRef]

30. O'Neill, R.D. Microvoltammetric Techniques and Sensors for Monitoring Neurochemical Dynamics in Vivo. A Review. *Analyst* **1994**, *119*, 767–779. [CrossRef]

31. Hong, Q.; Yang, L.; Ge, L.; Liu, Z.; Li, F. Direct-Laser-Writing of Three-Dimensional Porous Graphene Frameworks on Indium-Tin Oxide for Sensitive Electrochemical Biosensing. *Analyst* **2018**, *143*, 3327–3334. [CrossRef]

32. Nayak, P.; Kurra, N.; Xia, C.; Alshareef, H.N. Highly Efficient Laser Scribed Graphene Electrodes for On-Chip Electrochemical Sensing Applications. *Adv. Electron. Mater.* **2016**, *2*, 1600185. [CrossRef]

33. Xu, G.; Jarjes, Z.A.; Desprez, V.; Kilmartin, P.A.; Travas-Sejdic, J. Sensitive, Selective, Disposable Electrochemical Dopamine Sensor Based on PEDOT-Modified Laser Scribed Graphene. *Biosens. Bioelectron.* **2018**, *107*, 184–191. [CrossRef] [PubMed]

34. Krishnan, S.K.; Singh, E.; Singh, P.; Meyyappan, M.; Nalwa, H.S. A Review on Graphene-Based Nanocomposites for Electrochemical and Fluorescent Biosensors. *RSC Adv.* **2019**, *9*, 8778–8781. [CrossRef]

35. Gao, F.; Cai, X.; Wang, X.; Gao, C.; Liu, S.; Gao, F.; Wang, Q. Highly Sensitive and Selective Detection of Dopamine in the Presence of Ascorbic Acid at Graphene Oxide Modified Electrode. *Sens. Actuators B Chem.* **2013**, *186*, 380–387. [CrossRef]

36. Li, S.M.; Yang, S.Y.; Wang, Y.S.; Lien, C.H.; Tien, H.W.; Hsiao, S.T.; Liao, W.H.; Tsai, H.P.; Chang, C.L.; Ma, C.C.M.; et al. Controllable Synthesis of Nitrogen-Doped Graphene and Its Effect on the Simultaneous Electrochemical Determination of Ascorbic Acid, Dopamine, and Uric Acid. *Carbon* **2013**, *59*, 418–429. [CrossRef]

37. Ding, X.; Bai, J.; Xu, T.; Li, C.; Zhang, H.M.; Qu, L. A Novel Nitrogen-Doped Graphene Fiber Microelectrode with Ultrahigh Sensitivity for the Detection of Dopamine. *Electrochem. Commun.* **2016**, *72*, 122–125. [CrossRef]

38. Xu, T.Q.; Zhang, Q.L.; Zheng, J.N.; Lv, Z.Y.; Wei, J.; Wang, A.J.; Feng, J.J. Simultaneous Determination of Dopamine and Uric Acid in the Presence of Ascorbic Acid Using Pt Nanoparticles Supported on Reduced Graphene Oxide. *Electrochim. Acta* **2014**, *115*, 109–115. [CrossRef]

39. Randviir, E.P. A Cross Examination of Electron Transfer Rate Constants for Carbon Screen-Printed Electrodes Using Electrochemical Impedance Spectroscopy and Cyclic Voltammetry. *Electrochim. Acta* **2018**, *286*, 179–186. [CrossRef]

40. Yue, H.Y.; Huang, S.; Chang, J.; Heo, C.; Yao, F.; Adhikari, S.; Gunes, F.; Liu, L.C.; Lee, T.H.; Oh, E.S.; et al. ZnO Nanowire Arrays on 3D Hierachical Graphene Foam: Biomarker Detection of Parkinson's Disease. *ACS Nano* **2014**, *8*, 1639–1646. [CrossRef]

41. Mundaca-Uribe, R.; Bustos-Ramírez, F.; Zaror-Zaror, C.; Aranda-Bustos, M.; Neira-Hinojosa, J.; Peña-Farfal, C. Development of a Bienzymatic Amperometric Biosensor to Determine Uric Acid in Human Serum, Based on Mesoporous Silica (MCM-41) for Enzyme Immobilization. *Sens. Actuators B Chem.* **2014**, *195*, 58–62. [CrossRef]

42. Singh, S.P.; Li, Y.; Be'Er, A.; Oren, Y.; Tour, J.M.; Arnusch, C.J. Laser-Induced Graphene Layers and Electrodes Prevents Microbial Fouling and Exerts Antimicrobial Action. *ACS Appl. Mater. Interfaces* **2017**, *9*, 18238–18247. [CrossRef] [PubMed]

43. Jan, H.; Gul, R.; Andleeb, A.; Ullah, S.; Shah, M.; Khanum, M.; Ullah, I.; Hano, C.; Abbasi, B.H. A Detailed Review on Biosynthesis of Platinum Nanoparticles (PtNPs), Their Potential Antimicrobial and Biomedical Applications. *J. Saudi Chem. Soc.* **2021**, *25*, 101297. [CrossRef]
44. Kim, G.; Kim, H.; Kim, I.J.; Kim, J.R.; Lee, J.I.; Ree, M. Bacterial Adhesion, Cell Adhesion and Biocompatibility of Nafion Films. *J. Biomater. Sci. Polym. Ed.* **2009**, *20*, 1687–1707. [CrossRef] [PubMed]